

**You might find this additional information useful...**

---

A **corrigendum** for this article has been published. It can be found at:

<http://jn.physiology.org/cgi/content/full/95/6/3961>

**Supplemental material** for this article can be found at:

<http://jn.physiology.org/cgi/content/full/01141.2005/DC1>

**This article cites** 64 articles, 29 of which you can access free at:

<http://jn.physiology.org/cgi/content/full/95/4/2678#BIBL>

**This article has been cited by** 2 other HighWire hosted articles:

**Olfactory Coding With All-or-Nothing Glomeruli**

A. Koulakov, A. Gelperin and D. Rinberg  
*J Neurophysiol*, December 1, 2007; 98 (6): 3134-3142.

[\[Abstract\]](#) [\[Full Text\]](#) [\[PDF\]](#)

**GABAergic inhibition at dendrodendritic synapses tunes {gamma} oscillations in the olfactory bulb**

S. Lagier, P. Panzanelli, R. E. Russo, A. Nissant, B. Bathellier, M. Sassoe-Pognetto, J.-M. Fritschy and P.-M. Lledo

*PNAS*, April 24, 2007; 104 (17): 7259-7264.

[\[Abstract\]](#) [\[Full Text\]](#) [\[PDF\]](#)

**Updated information and services** including high-resolution figures, can be found at:

<http://jn.physiology.org/cgi/content/full/95/4/2678>

**Additional material and information** about *Journal of Neurophysiology* can be found at:

<http://www.the-aps.org/publications/jn>

---

This information is current as of October 21, 2008 .

# Circuit Properties Generating Gamma Oscillations in a Network Model of the Olfactory Bulb

Brice Bathellier,<sup>1,\*</sup> Samuel Lagier,<sup>1,\*</sup> Philippe Faure,<sup>2</sup> and Pierre-Marie Lledo<sup>1</sup>

<sup>1</sup>Laboratory of Perception and Memory and <sup>2</sup>Laboratory of Receptors and Cognition, Pasteur Institute, Centre National de la Recherche Scientifique Unité de Recherche Associée 2182, Paris, France

Submitted 28 October 2005; accepted in final form 21 December 2005

**Bathellier, Brice, Samuel Lagier, Philippe Faure, and Pierre-Marie Lledo.** Circuit properties generating gamma oscillations in a network model of the olfactory bulb. *J Neurophysiol* 95: 2678–2691, 2006. First published December 28, 2005; doi:10.1152/jn.01141.2005. The study of the neural basis of olfaction is important both for understanding the sense of smell and for understanding the mechanisms of neural computation. In the olfactory bulb (OB), the spatial patterning of both sensory inputs and synaptic interactions is crucial for processing odor information, although this patterning alone is not sufficient. Recent studies have suggested that representations of odor may already be distributed and dynamic in the first olfactory relay. The growing evidence demonstrating a functional role for the temporal structure of bulbar neuronal activity supports this assumption. However, the detailed mechanisms underlying this temporal structure have never been thoroughly studied. Our study focused on gamma (40–100 Hz) network oscillations in the mammalian OB, which is a form of temporal patterning in bulbar activity elicited by olfactory stimuli. We used computational modeling combined with electrophysiological recordings to investigate the basic synaptic organization necessary and sufficient to generate sustained gamma rhythms. We found that features of gamma oscillations obtained *in vitro* were identical to those of a model based on lateral inhibition as the coupling modality (i.e., low irregular firing rate and high oscillation stability). In contrast, they differed substantially from those of a model based on lateral excitatory coupling (i.e., high regular firing rate and unstable oscillations). Therefore we could precisely tune the oscillation frequency by changing the kinetics of inhibitory events supporting the lateral inhibition. Moreover, gradually decreasing GABAergic synaptic transmission decreased the degree of relay neuron synchronization in response to sensory inputs, both theoretically and experimentally. Thus we have shown that lateral inhibition provides a mechanism by which the dynamic processing of odor information might be finely tuned within the OB circuit.

## INTRODUCTION

The olfactory bulb (OB) plays a central role in processing and relaying olfactory information from the sensory organ to several central targets (Laurent et al. 2001; Lledo et al. 2005; Shepherd et al. 2004). After the pioneering studies of Lord Adrian (Adrian 1942, 1950), oscillations in the local field potential (LFP) of the OB are known to be a defining characteristic of sensory coding. From these studies, it has been suggested that synchronous fast oscillations in central sensory systems allow the formation of neural assemblies that represent sensory objects. In experiments performed on the olfactory processing circuitry, odor-triggered oscillations at a frequency

of 10–40 Hz in nonmammalian vertebrates and at both the beta band (15–30 Hz) and the low- and high-gamma bands (respectively 40–60 and 60–100 Hz) in mammals, are always seen. Although odor-evoked, temporally structured activity in the OB is well known to reflect odor coding and discrimination (Kay 2003; Laurent et al. 2001; Li and Hopfield 1989; Linster and Hasselmo 1997; Martin et al. 2004; Nusser et al. 2001; Urban and Sakmann 2002), the nature of the bulbar microcircuit elements that support these fast rhythms are still unclear. Computational models of the mammalian OB were previously designed (Freeman 1975, 1987; Li and Hopfield 1989; Linster and Hasselmo 1997) but were limited to the processing and coding of odorant information rather than the mechanisms of generating oscillations.

As in many cortical areas, there is a population of local interneurons in the OB, which is critical for shaping the dynamics of relay neurons, the mitral/tufted cells (MCs). These then convey information to higher integrative centers. MCs make various synaptic and nonsynaptic connections in the OB that mostly occur between dendrites (Schoppa and Urban 2003). These connections extend through multiple layers and integrate distinct microcircuits located either in glomeruli or in the external plexiform layer. Widespread interactions with the granule cells (GCs), which are local GABAergic interneurons, occur along the lateral dendrites of MCs (Lledo et al. 2005; Shepherd et al. 2004; Shipley and Ennis 1996). These dendrodendritic connections, which constitute the largest synaptic population of the OB, support both recurrent and lateral interactions (Schoppa and Urban 2003). Models have suggested for a long time that bulbar activity becomes rhythmically synchronized as a result of feedback interactions between MCs and GCs (Freeman 1975; Rall and Shepherd 1968). This is further supported by experimental studies demonstrating that local interneurons play a critical role in generating oscillatory activity in the antennal lobe of honeybees (Stopfer et al. 1997) and in the procerebral lobe of molluscs (Teyke and Gelperin 1999). Recent studies carried out in vertebrates showed that local inhibitory circuits are key elements to generating evoked gamma oscillations (Kay 2003; Lagier et al. 2004; Neville and Haberly 2003; Nusser et al. 2001). On the other hand, both theoretical (Migliore et al. 2005) and experimental studies (Christie et al. 2005; Schoppa and Westbrook 2002) recently suggested that direct excitation between MCs might be sufficient to synchronize them in the gamma range. Here, we have used a physiologically based network model of the OB combined with an experimental approach to investigate the precise

\* B. Bathellier and S. Lagier contributed equally to this work.

Address for reprint requests and other correspondence: P.-M. Lledo, Laboratory of Perception and Memory, CNRS URA 2182, 25 rue du Dr. Roux, 75724 Paris Cedex 15, France (E-mail: pmlledo@pasteur.fr).

The costs of publication of this article were defrayed in part by the payment of page charges. The article must therefore be hereby marked "advertisement" in accordance with 18 U.S.C. Section 1734 solely to indicate this fact.

synaptic organization and properties that drive the temporal patterns in OB activity. We propose that lateral inhibition plays a key role in generating sustained gamma oscillations and population synchrony.

## METHODS

### Single-neuron simulations

We used a single compartment that includes voltage-dependent currents described by Hodgkin–Huxley kinetics to model MC. These currents were fast transient ( $I_{Na}$ ) and persistent ( $I_{NaP}$ ) sodium currents, a delayed rectifier potassium current ( $I_{Kfast}$ ), and two transient potassium currents (fast inactivating  $I_{Ka}$ , slow inactivating  $I_{Ks}$ ). Synaptic ( $I_{syn}$ ), input ( $I_{input}$ ), and noise ( $I_{noise}$ ) currents were added to the voltage-dependent currents (Eq. A1 in the APPENDIX). Values for passive membrane properties ( $C_m = 0.01$  F/m<sup>2</sup> and  $R_m = 10$   $\Omega$ m<sup>2</sup>) and the leak potential ( $E_L = -66.5$  mV) were chosen from Bhalla and Bower (1993). Values for Na ( $E_{Na} = 45$  mV,  $g_{Na} = 500$  S/m<sup>2</sup>) and Kfast ( $E_{Kfast} = -70$  mV,  $g_{Kfast} = 500$  S/m<sup>2</sup>) currents were also taken from Bhalla and Bower (1993) except that their activation and inactivation curves were shifted by  $-8$  mV to lower the spike threshold in accordance with previous results (Desmaisons et al. 1999). The Ka current ( $E_{Ka} = -70$  mV,  $g_{Ka} = 100$  S/m<sup>2</sup>) was adapted from Wang et al. (1996) and its kinetics were taken from the Senselab databank (<http://senselab.med.yale.edu>). Ks ( $E_{Ks} = -70$  mV,  $g_{Ks} = 310$  S/m<sup>2</sup>) and NaP ( $E_{NaP} = 45$  mV,  $g_{NaP} = 1.1$  S/m<sup>2</sup>) currents were adapted from Wang (1993). Each cell received Gaussian white noise with a variance equal to 0.12 A/m<sup>2</sup>. All voltage-dependent current amplitudes were varied by  $\pm 20\%$  among the neurons in our models. Further details are presented in the APPENDIX and in Supplementary Fig. 1.<sup>1</sup>

### Synaptic current simulations

Conductance kinetics were modeled by a delayed difference of two exponential functions of time  $t$

$$g(t) = M_{\tau_r, \tau_d} [\exp(-t/\tau_d) - \exp(-t/\tau_r)] \quad (1)$$

where  $\tau_r$  and  $\tau_d$  are the rise time and decay time of synaptic currents, respectively.  $M_{\tau_r, \tau_d}$  is a factor of  $\tau_r$  and  $\tau_d$ , such that the maximum of  $g(t)$  (with respect to time) is equal to 1. The resulting current is given by

$$I_{syn} = G_{syn}(V - E_{reversal})g(t) \quad (2)$$

where  $G_{syn}$  is the maximal synaptic conductance. Reversal potentials were 0 mV for excitatory (glutamatergic) synapses (including lateral and recurrent excitation, as well as olfactory nerve inputs) and  $-70$  mV for inhibitory (GABAergic) synapses. All synaptic currents were induced by MC presynaptic spikes (interneurons were not modeled explicitly), with a latency  $\tau_p$ , ranging from 0 to 3 ms (Figs. 1 to 4). Throughout this study, except for the result presented in Fig. 8A, lateral inhibition was modeled with  $\tau_d = 20$  ms,  $\tau_r = 3$  ms, and  $\tau_i = 2$  ms; recurrent inhibition with  $\tau_d = 50$  ms,  $\tau_r = 1$  ms, and  $\tau_i = 1$  ms; and lateral excitation with  $\tau_d = 10$  ms,  $\tau_r = 0.5$  ms, and  $\tau_i = 1.4$  ms (see also Fig. 8 and Table 1).

For lateral and recurrent inhibition, we used a model of asynchronous release (Figs. 7 and 8). At each step of the simulation an event was generated according to the value of a probability density  $p(t)$ . The events were modeled as transient conductance openings [the difference of two exponentials with  $\tau_d = 10$  ms and  $\tau_r = 0.5$  ms, taken from Castillo et al. (1999)]. In the absence of spikes, the probability had a constant value ( $p_0$ ), which produced spontaneous synaptic activity. In response to a spike, a function was added to  $p(t)$  to transiently increase the number of incoming synaptic events. Two different decay times

were used to describe the probability for recurrent ( $\tau_d = 150$  ms) and lateral inhibition ( $\tau_d = 50$  ms). The rise time and latency were both set to 0.5 ms. Finally, excitatory olfactory nerve (ON) inputs into glomeruli were modeled either by a difference of two exponentials ( $\tau_d = 300$  ms and  $\tau_r = 50$  ms) or by a step function (constant inputs).

### Network architecture

The network of MCs used for the simulations was a matrix of  $10 \times 10$  cells. The coupling amplitude (either the magnitude of the conductance change or the probability of inhibitory events) between two MCs was dependent on their distance  $d$  (expressed as cell number). The spatial profile of connectivity was Gaussian

$$G(d) = g_c \exp(-d^2/L^2) \quad (3)$$

with a typical length  $L$  of four cells for both lateral excitation and lateral inhibition ( $L = 5$  for the model including asynchronous release) and  $g_c$  as the amplitude of lateral inhibition or excitation. We accounted for variability in coupling strength, by randomly choosing the coupling amplitudes between cell  $i$  and  $j$  [i.e.,  $g_{syn}(i, j)$ ] such that  $0 < g_{syn}(i, j) < G(d)$  with a uniform probability. Recurrent inhibition varied from cell to cell ( $\pm 50\%$  of its average value). In simulated MCs, we randomly varied the amplitude of each intrinsic current from cell to cell ( $\pm 50\%$  of their average values). This gave a large variability in cell excitability such that neurons exhibited a broad range of firing rates even when the same input amplitude was given to all cells. All the parameters used are presented in Table 1.

### Simulated local field potential

We constructed a simulated LFP (sLFP) by filtering the mean membrane potentials across all 100 cells. We used this as a parameter to assess network oscillations and synchrony, from which we could extract the frequencies of rhythmic activities. Filtering was carried out numerically using a band-pass Bessel filter (10–100 Hz) and was done twice (forward and backward) to remove artificial phase lags.

### Simulation procedure

All network simulations were performed using a fourth-order Runge–Kutta integration method. The time steps were either 10, 20, or 40  $\mu$ s. The results were not affected by changing this parameter. The input onset was 200 ms after the start of the simulation to allow the simulated cells to stabilize. The C++ source code was compiled on an Intel PC using a DEV C++ compiler (version 4.9.7.0). A simulation of 1 s of network activity took between 7 to 22 min of CPU time depending on the number of synaptic connections. Visualization and analysis of the results were carried out with Elphy software (G Sadoc, CNRS, Gif-sur-Yvette, France).

### Synchronization and oscillation indices

The synchronization index is equal to

$$1/N \sqrt{\sum_{i=1}^N [\sin^2(\varphi_i) + \cos^2(\varphi_i)]} \quad (4)$$

where  $\varphi_i$  denotes the phase of each spike in the network with respect to local maxima in the experimental/simulated LFP (Fig. 2F). It corresponds to the length of the phase distribution vector and ranges from 0 to 1. The oscillation index (ranging from 0 to 1) corresponds to the amplitude of the secondary peak of the LFP autocorrelation, normalized by the mean and variance of the signal (Fig. 2E). The position of the secondary peak of the autocorrelograms was used to determine the oscillation frequency. In the simulated network, when inputs were step functions, the analysis was performed over a 700-ms time range, and when the inputs varied with time (as in slice recordings), the analysis was performed over a 200-ms time range.

<sup>1</sup> The Supplementary Material for this article (a figure) is available online at <http://jn.physiology.org/cgi/content/full/01141.2005/DC1>.

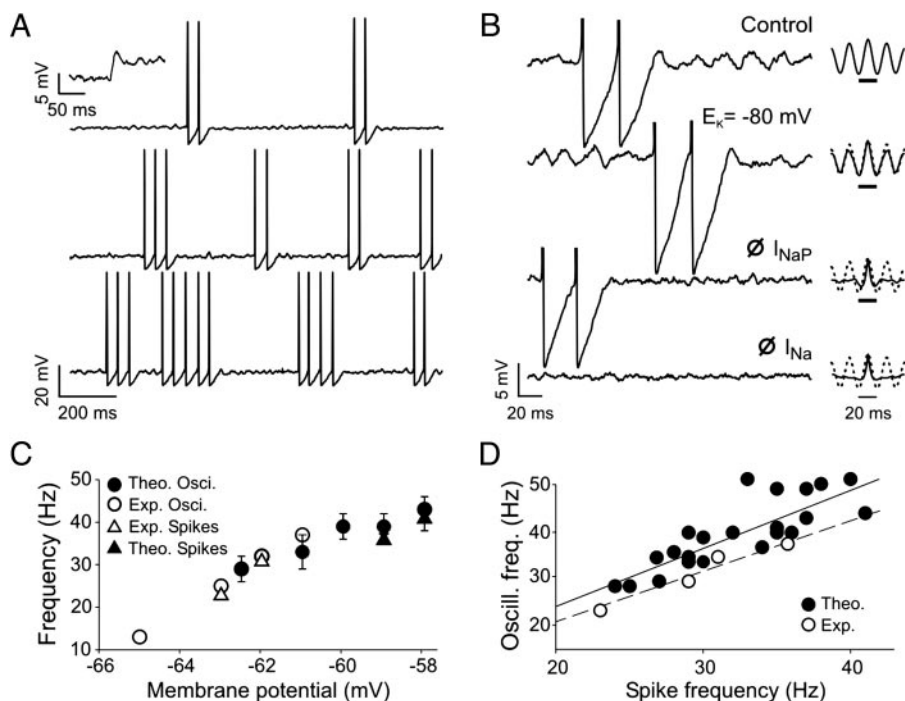


FIG. 1. Mitral cell spiking activity and subthreshold membrane potential oscillations. *A*: firing patterns of simulated mitral/tufted cells (MCs) in response to constant DC current injections (respectively 0.02, 0.025, and 0.03 A/m<sup>2</sup> from top to bottom). Note the sag at stimulation onset (*inset*). *B*, left: simulated MC membrane potential traces undergoing modification of their voltage-dependent conductances. Subthreshold oscillations were affected only after removing the persistent sodium current ( $\emptyset I_{NaP}$ ), or all sodium currents ( $\emptyset I_{Na}$ ), but not by lowering ( $-5$  mV) the potassium equilibrium potential ( $E_K = -80$  mV). *Right*: autocorrelation of the membrane potential corresponding to the left traces, with dashed lines representing traces before modifications. *C*: voltage dependency of the oscillation frequency (circles) and spike frequency (triangles) from recorded (open symbols) and simulated (closed symbols) MCs. *D*: relationship between spike frequency and subthreshold oscillation frequency. Values were from experiments (open symbols) or from a model in which random combinations of  $\pm 20\%$  variations in the magnitude of voltage-activated currents were introduced (closed symbols). Linear regressions have slopes of 1.1 and 1.0 for the model and experimental data, respectively.

### Experimental procedure

OB slices were prepared from 4- to 6-wk-old C57Bl/6 mice and electrophysiological recordings were carried out as previously described (Lagier et al. 2004). For extracellular single-unit recordings, thick-walled glass pipettes (Clark Electromedical Instruments, Reading, UK) were pulled with a custom vertical puller and filled with 2 M NaCl (DC resistance 5–15 M $\Omega$ ). Single-unit recordings were amplified using an Iso-DAM8 differential amplifier (World Precision Instruments, Hertfordshire, UK), filtered (0.3–3 kHz), and sampled at 20 kHz. MCs were identified by their peristimulus time histogram (PSTH) profile and their phase locking to LFP oscillations (see Fig. 5 and Lagier et al. 2004).

### Statistical analysis

We analyzed the frequency distributions using the Kolmogorov–Smirnov test, the pharmacological experiments using Student's *t*-test, and the spike-phase distributions using three different circular statistical tests (Rayleigh, Watson, and Kuiper) (Lagier et al. 2004). The level of significance was set to  $P = 0.05$ . All results are expressed as means  $\pm$  SE.

## RESULTS

### Minimal intrinsic properties reproducing mitral/tufted cell physiology

From the literature, we selected a minimal set of parameters (Bhalla and Bower 1993; Davison et al. 2000; Wang 1993) required to reproduce the characteristic properties of MCs, that is, a delayed onset of firing (e.g., Balu et al. 2004; Chen and Shepherd 1997) and repetitive firing of clustered action potentials separated by periods of subthreshold oscillations in response to DC current injection (e.g., Balu et al. 2004; Chen and Shepherd 1997; Desmaisons et al. 1999). These characteristics arise from intrinsic membrane properties because they persist in the presence of ionotropic glutamate and  $\gamma$ -aminobutyric acid (GABA) receptor blockers (Balu et al. 2004; Desmaisons et al. 1999). Furthermore, the presence of A-type potassium

(Ka; Wang et al. 1996) and slow-inactivating potassium currents (Ks; Balu et al. 2004) in MCs can explain both delayed firing onset and spike clustering (Fig. 1A).

As indicated by their sensitivity to tetrodotoxin (TTX) (Desmaisons et al. 1999), subthreshold oscillations could be generated in MCs by the interaction between a persistent sodium current (NaP), Ks, and intrinsic noise. The combination of NaP and Ks is known to produce a resonance of the membrane voltage in some neurons (Hutcheon and Yarom 2000). This resonance property, combined with intrinsic noise, generates irregular membrane subthreshold oscillations (Fig. 1A). The peak of resonance, and therefore the frequency of subthreshold oscillations, depends on the activation time constant of Ks (Richardson et al. 2003), which we set here to 10 ms.

The suppression of all Na<sup>+</sup> currents abolishes the subthreshold oscillations (Desmaisons et al. 1999). We found the same in our model, with either all Na<sup>+</sup> currents being suppressed or the NaP current being selectively suppressed (Fig. 1B). By contrast, when we changed the K<sup>+</sup> driving force in our model (Fig. 1B) the subthreshold oscillations were not affected, which has also been seen experimentally (Desmaisons et al. 1999). We also found that the frequency of oscillations and the instantaneous intraburst spike frequency were highly correlated in our model (Fig. 1C), which has also been reported experimentally (Desmaisons et al. 1999). However, in our model, the frequency of the membrane potential oscillations was 10% faster than the firing frequency, whereas the experimental oscillation frequency was tightly linked with the firing frequency (Fig. 1D). Nevertheless, the good agreement between our simulation and experimental data suggested that our simple model cell was capturing the main features of MCs recorded in slices.

### Generating oscillations in a simplified olfactory bulb circuit

We designed a model of OB local circuitry containing 100 heterogeneous MCs (see METHODS) and receiving ON inputs.

TABLE 1. Parameters of MC network architecture

General Cell Properties				
$C_m$	Membrane capacitance	Eq. 1*	0.01 F/m <sup>2</sup>	Bhalla and Bower 1993
$R_m$	Membrane resistance	Eq. 1	10 $\Omega$ m <sup>2</sup>	Bhalla and Bower 1993
$E_r$	Reverse leak potential	Eq. 1	-66.5 mV	Bhalla and Bower 1993
Conductances			<i>Na</i>	
$M$	Number of activating gates	Eq. 2	3	Bhalla and Bower 1993
$H$	Number of inactivating gates	Eq. 2	1	Bhalla and Bower 1993
$g_{max}$	Averaged maximal conductance	Eq. 2	500 S/m <sup>2</sup>	Bhalla and Bower 1993
$E$	Reversal potential	Eq. 2	45 mV	Bhalla and Bower 1993
$\tau_m$	Activation time constant	Eq. 3	Function (see Bhalla and Bower 1993)	
$\tau_h$	Inactivation time constant	Eq. 4	Function (see Bhalla and Bower 1993)	
$m_4$	Steady-state activation	Eq. 3	Function (see Bhalla and Bower 1993)	
$h_4$	Steady-state inactivation	Eq. 4	Function (see Bhalla and Bower 1993)	
Synaptic transients			<i>Excitation (auto and lateral)</i>	
$\tau_l$	Latency		1.4 ms	Urban and Sakmann 2002
$\tau_r$	Rise time constant	Eq. 7	0.5 ms	Schoppa and Westbrook 1999
$\tau_d$	Decay time constant	Eq. 7	10 ms	Brunel and Wang 2003
$E_{reversal}$	Reversal potential	Eq. 8	0 mV	Varied, data not shown
$g_{syn}$	Maximum conductance	Eq. 8	0-1.6 S/m <sup>2</sup>	Brunel and Wang 2003
				Varied in Fig. 3
		<i>NaP</i>		<i>Kfast</i>
1		Wang 1993	2	Bhalla and Bower 1993
0 (no inactivation)		Wang 1993	1	Bhalla and Bower 1993
1.1 S/m <sup>2</sup>		Bhalla and Bower 1993	500 S/m <sup>2</sup>	Bhalla and Bower 1993
45 mV		Bhalla and Bower 1993	-70 mV	Bhalla and Bower 1993
0 (instantaneous activation)		Wang 1993		Function (see Bhalla and Bower 1993)
Not used (no inactivation)		Wang 1993		Function (see Bhalla and Bower 1993)
Function (see Wang 1993)		Wang 1993		Function (see Bhalla and Bower 1993)
Not used (no inactivation)		Wang 1993		Function (see Bhalla and Bower 1993)
		<i>Ka</i>		<i>Ks</i>
1	~		1	~
1	~		1	~
100 S/m <sup>2</sup>	#		310 S/m <sup>2</sup>	#
-70 mV		Bhalla and Bower 1993	-70 mV	Bhalla and Bower 1993
See METHODS		Wang 1996	10	#
See METHODS		Wang 1996	See METHODS	Wang 1993
See METHODS		Wang 1996	See METHODS	Wang 1993
See METHODS		Wang 1996	See METHODS	Wang 1993
		<i>Recurrent inhibition</i>		<i>Lateral inhibition</i>
1 ms	Varied, data not shown		2 ms	Varied in Fig. 8
1 ms	Varied, data not shown		3 ms	Varied in Fig. 8
50 ms	Varied, data not shown		20 ms	Varied in Fig. 8
-70 mV		Brunel and Wang 2003	-70 mV	Brunel and Wang 2003
0-64 S/m <sup>2</sup>		Varied in Fig. 3	0-32 S/m <sup>2</sup>	Varied in Fig. 3
Connectivity				
$L$	Characteristic distance	Eq. 9	4-5 cells	Varied, data not shown
$G(d)$	Connection probability	Eq. 9	See METHODS	Function arbitrarily chosen
Probabilistic synaptic description				
$P_{max\ recurrent}$	Maximum transient probability		7.5 ms <sup>-1</sup>	Inferred from Isaacson and Strowbridge 1998
$P_{max\ lateral}$	Maximum transient probability		0.75 ms <sup>-1</sup>	Inferred from Isaacson and Strowbridge 1998
$P_o$	Basal probability		0.0125 ms <sup>-1</sup>	Castillo et al. 1999
$\tau_l$	Latency		0.5 ms	Inferred from Isaacson and Strowbridge 1998
$\tau_r$	Rise time constant		0.5 ms	Inferred from Isaacson and Strowbridge 1998
$\tau_d$	Decay time constant (for rec. inh.)		150 ms	Inferred from Isaacson and Strowbridge 1998
$\tau_d$	Decay time constant (for lat. inh.)		50 ms	Inferred from Isaacson and Strowbridge 1998
Individual uIPSC				
$\tau_l$	Latency		0 ms	No latency needed
$\tau_r$	Rise time constant		0.5 ms	Brunel and Wang 2003
$\tau_d$	Decay time constant		10 ms	Castillo et al. 1999
$g_{syn}$	Maximum conductance		0-0.06 S/m <sup>2</sup>	Varied in Fig. 5

\*Values from this column refer to equations in METHODS and the APPENDIX. #, these parameters control membrane subthreshold oscillations. In the absence of experimental values, we chose these values to fit subthreshold oscillation properties with experimental data. ~, <http://senselab.med.yale.edu>.

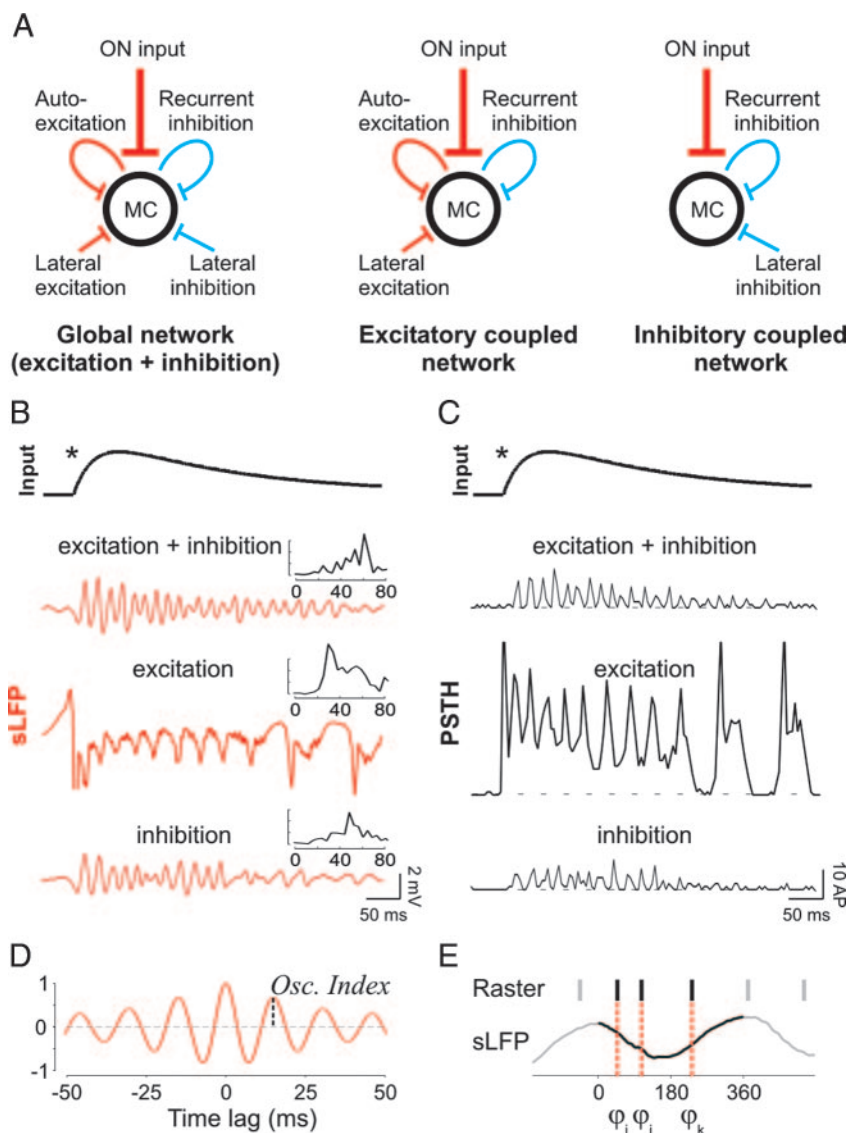


**FIG. 2.** Recurrent and lateral couplings between MCs in the olfactory bulb (OB) network model. **A:** architectural features of bulbar modeled networks used in the study. *Red* and *blue* traces represent excitatory and inhibitory connections, respectively. Note that sensory entry [olfactory nerve (ON) input] was homogeneously distributed within the network. Models were made from a matrix of  $10 \times 10$  neurons having different couplings. One model contained all described connections (global network), the second did not feature lateral inhibitory connections (E-network), whereas the last lacked excitatory connections (I-network). **B:** sensory input (*top* trace) induced  $\gamma$  oscillations of simulated local field potentials (sLFPs) in 3 different conditions: both lateral excitation and inhibition are implemented together with recurrent inhibition (*top*), only lateral excitation with recurrent inhibition is implemented (*middle*), and only lateral and recurrent inhibition are implemented (*bottom*). All conditions led to oscillations in the  $\gamma$  range. *Insets:* plots of the fast Fourier transform of the sLFP with arbitrary power units. **C:** peristimulus time histograms (PSTHs) of MC responses triggered by the same sensory input (*top*) and under the same 3 conditions as in **C**. **D:** normalized autocorrelation of the sLFP exemplifying the determination of the oscillation index (defined as the height of the first secondary peak). **E:** one oscillation cycle of the sLFP illustrating the determination of the spike phase. Spike phases ( $\varphi$ ) were computed with respect to their timing compared with the position of 2 consecutive maxima of the sLFP (defining 0 and  $360^\circ$  of phase). In this example  $\varphi_i$ ,  $\varphi_j$ , and  $\varphi_k$  are 47, 108, and  $233^\circ$ , respectively. Phases were then used to compute the synchronization index.

This network model includes the main synaptic interactions (lateral excitation and inhibition), and recurrent action (auto-excitation and recurrent inhibition). In a first set of simulations (Figs. 2–6), all synaptic currents were approximated as their averaged time course (smooth functions) using a difference of two exponentials. This is appropriate for lateral excitation and we derived our kinetic constants from their excitatory postsynaptic potential (EPSP) time courses (Urban and Sakmann 2002). However, for lateral inhibition, this approximation masks two different aspects of the coupling. First, lateral inhibition between MCs is the sum of small asynchronous inhibitory postsynaptic currents (IPSCs) rather than being a simple exponentially decaying event. Second, it is not a direct coupling (like lateral excitation) but is mediated by GABAergic interneurons through dendrodendritic synapses. We omitted interneurons from our model circuit (but kept their resulting synaptic interactions) because the integration properties of bulbar interneurons are still unclear despite numerous recent studies (Egger et al. 2005; Hall and Delaney 2002; Isaacson and Strowbridge 1998; Murphy et al. 2005; Pinato and Midtgard 2005; Schoppa and Westbrook 1999). A consequence of

such a simplification is that the inhibitory coupling parameters are not derived from a real biophysical system. Thus our approach holds only as long as the conclusions drawn do not depend on a particular set of values chosen for these parameters. Therefore to be consistent, we analyzed systematic variations of amplitudes and time constants of lateral and recurrent inhibition and we draw our conclusions only from general observations. We also systematically varied the lateral- and autoexcitation parameters to verify that their initial values were not biasing the simulation outputs.

Our global network model (containing both inhibitory and excitatory coupling; Fig. 2A, *left*) responded to an excitatory input current (*top* traces in Fig. 2, B and C) by generating oscillations in the gamma band observed in both the sLFP (Fig. 2B) and the PSTH (Fig. 2C). We designed two other models to dissociate the respective properties from the two coupling modalities and to determine by comparison which one is dominant in the OB. One model had couplings that were only excitatory (E-network, Fig. 2A, *middle*); the other had couplings that were only inhibitory (I-network, Fig. 2A, *right*). In both I- and E-networks, recurrent inhibition was present. In

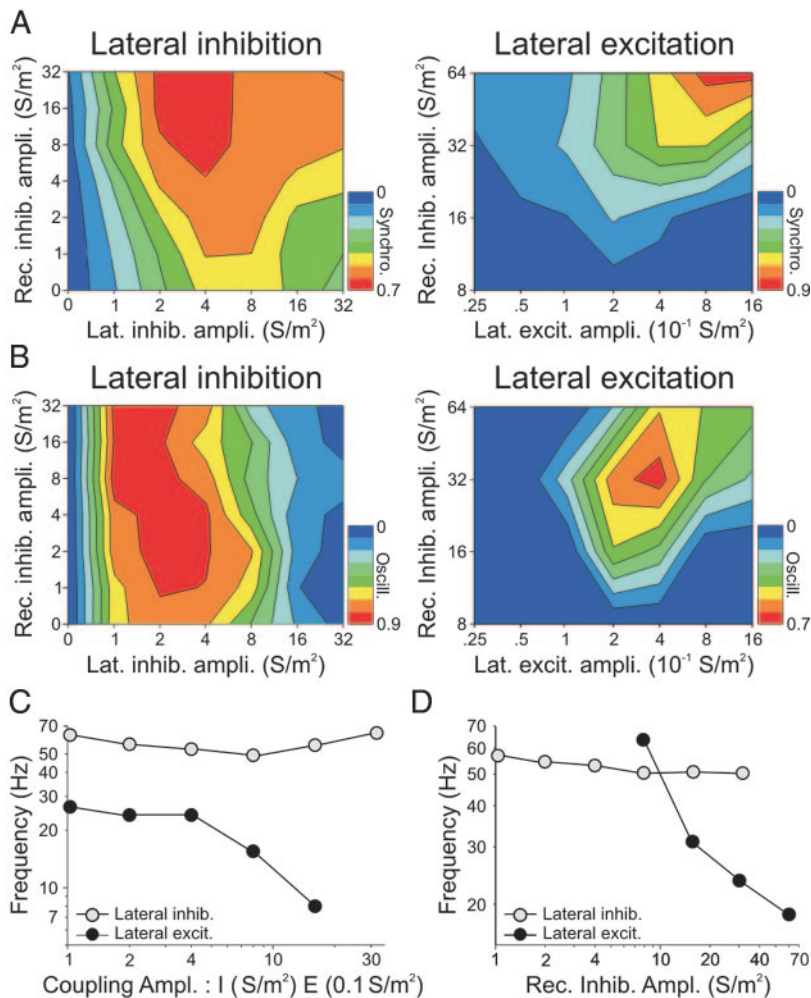


FIG. 3. Coupling types dramatically influence network stability. *A*: plot of the synchronization index (S.I., color scale) with respect to variations in the amplitude of recurrent inhibition and lateral inhibitory couplings (*left*) and in the amplitude of recurrent inhibition and lateral excitatory couplings (*right*). *B*: same plots as in *A* but for the oscillation index (O.I.). Note the stability of the inhibitory-coupled network compared with its excitatory-coupled counterpart. *C* and *D*: dependency of the frequency of network oscillations on the strength of coupling (*C*) and on the strength of recurrent inhibition (*D*) in lateral inhibitory-coupled (gray circles) and lateral excitatory-coupled (black circles) networks. In *C*, recurrent inhibition was set to 4 and 32 S/m<sup>2</sup> for lateral inhibitory-coupled and lateral excitatory-coupled networks, respectively. In *D*, lateral inhibition was set to 4 S/m<sup>2</sup> and lateral excitation to 0.4 S/m<sup>2</sup>.

these two models gamma frequencies were also generated for a given set of parameters (Fig. 2, *B* and *C*, *middle* and *bottom traces*). The rest of the study systematically investigated the oscillation properties caused by lateral inhibition and lateral excitation, while keeping the amplitude of sensory inputs constant in time. We looked at four quantification parameters (see METHODS): an oscillation index (O.I.; Fig. 2*D*), a synchrony index (S.I.; Fig. 2*E*), the oscillation frequency, and the mean firing rate of the network.

#### Inhibition- versus excitation-coupled network models

We assessed the stability of the synchrony for variations in the recurrent inhibition strength (which controls MC excitability) and lateral coupling strength (inhibition for the I-network in Fig. 3*A*, *left*, and excitation for the E-network in Fig. 3*A*, *right*). In the I-network, we found that a wide range of parameters (lateral and recurrent inhibition between 1 and 32 S/m<sup>2</sup>) led to high synchronization indices (S.I. >0.4; Fig. 3*A*, *left*, predominance of warm colors). By contrast, in the E-network, high levels of synchronization (S.I. >0.4) were limited to a small set of parameters (Fig. 3*A*, *right*, predominance of cold colors) that corresponded to a combination of strong recurrent inhibition (>32 S/m<sup>2</sup>) and strong lateral excitation (>0.4 S/m<sup>2</sup>, Fig. 3*A*, *right*). We observed a similar stability with oscillations: the E-network was more sensitive than the

I-network to changes in both lateral and recurrent inhibition amplitudes (Fig. 3*B*).

We analyzed the frequency of oscillations to determine the stability of the I-network (Fig. 3, *C* and *D*). For variations in both lateral and recurrent inhibition, the frequency of oscillation in the I-network remained stable (between 50 and 70 Hz), whereas it varied considerably in the E-network (from 67 to 19 Hz when increasing the recurrent inhibition amplitude from 10 to 70 S/m<sup>2</sup>; Fig. 3*D*). These results demonstrate that the I-network provides more stable oscillations than the E-network.

#### Frequency of oscillations and firing rates

We analyzed the firing pattern of MCs to differentiate the oscillatory states in the I- and E-networks. We found that the oscillatory activity in the E-network always had mean firing rates equal to or higher than the oscillation frequency (Fig. 4*B1*). The MCs fired at least once during each oscillation cycle (see Fig. 4*B2*) and the network oscillations arose from synchronization of all MCs. This spiking behavior was observed for all the MC and network parameters we tested. In particular, even after reducing MC excitability by a drastic reduction in sodium conductance [from 500 S/m<sup>2</sup> taken from a theoretical model in Bhalla and Bower (1993) to 90 S/m<sup>2</sup> given by Bischofberger and Jonas (1997) who effectively measured

sodium conductance in the primary dendrite of MCs], no cycle skipping of the MC spike was observed (see Supplementary Fig. 1). Therefore we conclude that only the lateral inhibitory model reproduces the skips in MC firing. Similarly, changes in the time constants of the lateral excitation did not lead to a state where MCs were firing at a lower rate than the oscillation frequency (see Supplementary Fig. 2). In all cases, individual spiking frequency came from alternating phases of inhibition (caused by a spike in the cell) and excitation (coming from ON input and from surrounding activity). This required an excitatory coupling strong enough to make all neurons fire at the same time (synchronization of the individual oscillators; see for example Van Vreeswijk et al. 1994), and an inhibition strong enough to silence each neuron afterward. Therefore the balance between excitation (including input strength) and inhibition strictly determined the oscillation frequency (Fig. 3, *C* and *D*). By contrast, in the I-network, the individual neurons fired at a lower rate than the global oscillation frequency (Fig.

4*A1*), with the individual neurons not firing on each oscillation cycle (Fig. 4*A2*). Therefore in this model, the coupling periodically modulates the instantaneous firing rate of the network rather than synchronizing the oscillating neurons. Thus oscillations in the I- and E-networks seemed to occur through two different mechanisms.

Some of the dynamic properties of these mechanisms could be studied using electrophysiological experiments. In particular, our first set of simulations yielded one simple prediction. A low individual firing rate in a network (e.g., Fig. 4*A2*) suggests that lateral inhibition dominates lateral excitation. By contrast, a high individual firing rate, equal to the oscillation frequency (e.g., Fig. 4*B2*), suggests that lateral excitation dominates for both oscillation and synchronization. Therefore we studied electrophysiological recordings in OB slices to investigate which coupling type predominates for generating gamma oscillations. First, we recorded ON-induced LFP oscillations using simultaneous MC single-unit recordings (Fig. 4*C*). The

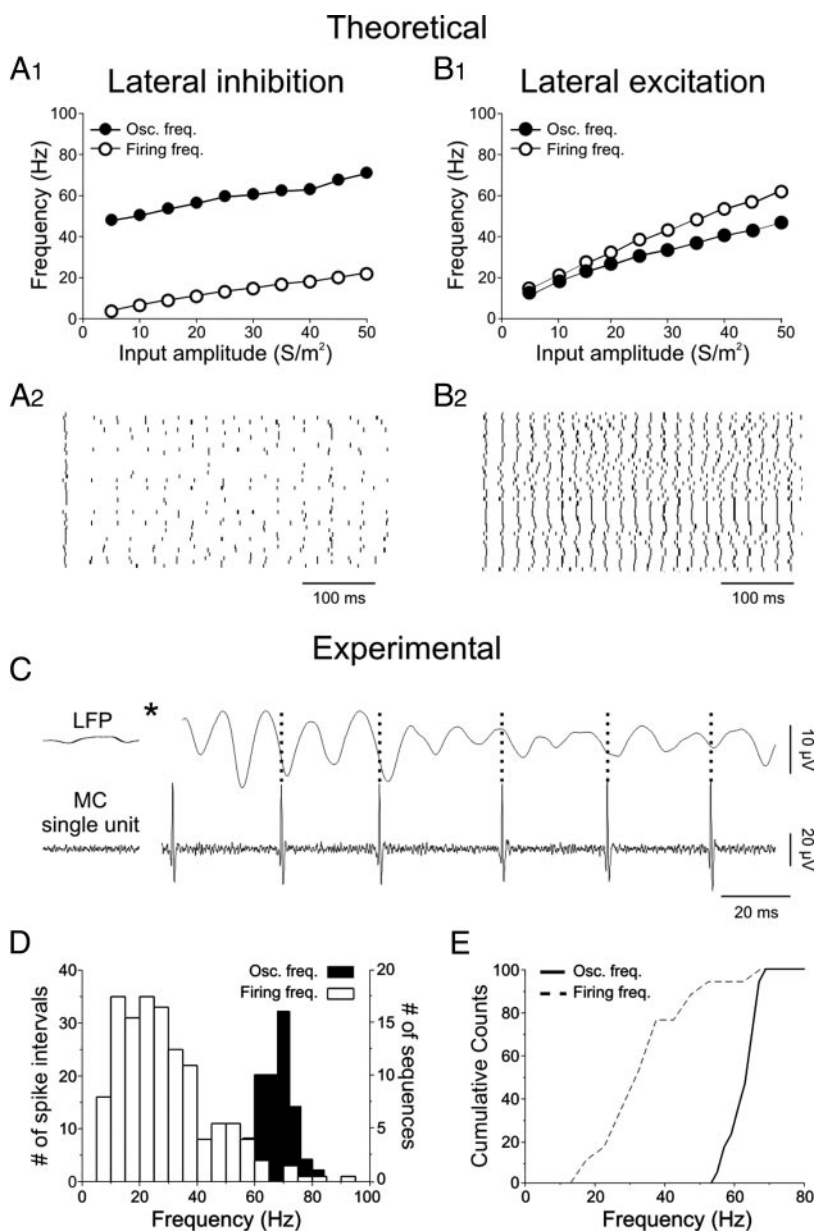


FIG. 4. Frequency of network oscillations and MC firing rate depend on the amplitude of sensory input. *A1*: plot of individual firing rate (open circles) and network oscillation frequency (filled circles) with respect to the magnitude of the mean input received per cell, in a lateral inhibitory-coupled network and (*B1*) a lateral excitatory-coupled network. *A2*: raster plots of the firing patterns of 100 simulated MCs in the inhibitory-coupled network and (*B2*) in the excitatory-coupled network. Each bar represents an action potential. In *A1* and *A2*, lateral and recurrent inhibition amplitudes were set to 4 and 16  $S/m^2$ , respectively. In *B1* and *B2*, lateral excitation and recurrent inhibition amplitudes were set to 0.8 and 64  $S/m^2$ , respectively. *C*: simultaneous LFP and MC single-unit recording. Note that the recorded MC did not fire on each LFP cycle and, when it did, spikes occurred during the descending phase of the oscillation. The star indicates the time of the ON stimulation. *D*: histograms of instantaneous firing (white columns) and LFP oscillation (black columns) frequencies recorded in a single experiment. A single MC was recorded in this case ( $n = 50$  values of LFP frequency,  $n = 245$  values of instantaneous firing frequency,  $P < 0.001$  with Kolmogorov–Smirnov test). *E*: cumulative plots of instantaneous firing and LFP oscillation frequencies recorded from 16 experiments ( $P < 0.001$  with Kolmogorov–Smirnov test).

instantaneous firing frequencies (Fig. 4D, white columns,  $n = 245$ ) almost never overlapped LFP oscillation frequencies (black columns,  $n = 50$ ; Kolmogorov–Smirnov test,  $P < 0.001$ ). On average, the MC firing frequency was  $35.9 \pm 3.2$  Hz, whereas the mean LFP oscillation was  $63.1 \pm 1.0$  Hz (Fig. 4E;  $n = 16$ ; Kolmogorov–Smirnov test,  $P < 0.001$ ). All neurons used in this analysis showed a sustained firing rate and a phase locking to the LFP (Fig. 5, for an individual cell in A and for all the recorded cells in B). These results showed that lateral inhibition was the major coupling required to generate gamma oscillations in the OB network. Therefore we focused our analysis on the I-network.

#### Determining the oscillation frequency in the I-network

We investigated the properties of oscillations in the I-network by independently varying the inhibitory coupling event time constants (around the reference values given in METHODS) while keeping the total charge of the event constant to minimize changes in the mean network firing rate. We always kept the global onset of the event (i.e., latency + rise time)  $>2$ – $3$  ms to maintain the oscillation frequency in the gamma range. For shorter onset times, the frequencies were  $>80$  Hz (data not shown; see Brunel and Wang 2003). Rise time constant and latency both had the same independent effect on oscillation frequency while preserving oscillations and MC synchrony. Indeed, increasing rise time (from 0.2 to 5 ms) caused the oscillation frequency to continually decrease (from 73.4 to 46.1 Hz; Fig. 6A, left), without greatly affecting synchrony and oscillation indices (O.I. ranged from 0.76 to 0.58; S.I. from 0.52 to 0.69; Fig. 6A, right). Similarly, increasing the latency of the coupling event (from 0.2 to 5 ms) caused a steady decrease in frequency (from 79.0 to 33.5 Hz; Fig. 6B, left), again without greatly affecting the synchrony and oscillation indices (O.I. ranging from 0.62 to 0.66; S.I. from 0.49 to 0.71; Fig. 6B, right). By contrast, changing the decay time did not greatly affect the oscillation frequency but did affect the

synchrony and oscillation indices. For decays  $>5$  ms, the oscillation frequency was unchanged (between 50 and 55 Hz, Fig. 6C, left) whereas the MC synchrony decreased for decays  $>40$  ms (S.I. from 0.65 to 0.24; Fig. 6C, right). Likewise, the oscillation quality was reduced with both short ( $<20$  ms) and long decays ( $>80$  ms; O.I.  $<0.35$  in both cases; Fig. 6C, right). These results demonstrate the high sensitivity of the I-network oscillatory dynamic to the temporal features of lateral inhibitory coupling. Furthermore, the frequency is crucially determined by the onset (i.e., latency and rise time) of the coupling rather than by its duration (i.e., decay time). Given that the rise time of lateral inhibition coupling is strongly dependent on the modalities of GABA release, we developed a simple model to check the influence of the sum of multiple individual IPSCs on the time course of global IPSCs.

#### Modeling the temporal features of inhibitory synaptic events in mitral/tufted cells

Lateral and recurrent inhibition can be considered as a long-lasting global increase in the frequency of vesicular GABA release. Thus in our second model, IPSCs received by MCs were considered as the sum of unitary IPSCs (Fig. 7, A–C, black traces). In a given MC, activity transiently changed the probability of receiving unitary IPSCs (Fig. 7, A–C, red traces). We tuned parameters to the particular properties of GC to MC inhibition [i.e., decay of unitary IPSCs of 10 ms, see Castillo et al. (1999); ratio of lateral to reciprocal inhibition of 0.1, see Isaacson and Strowbridge (1998)]. We focused on this type of synapse because it is the main inhibitory connection involved in generating gamma oscillations (Lagier et al. 2004).

We observed that the rise time of the global coupling event (Fig. 7C, black trace) was large (around 8–10 ms) as a result of the gradual summing of IPSCs despite the fast rise time of the individual IPSCs (0.5 ms) and of the release probability (0.5 ms). Thus the asynchronous GABA release time constants were in the range of parameters giving rise to oscillations in the

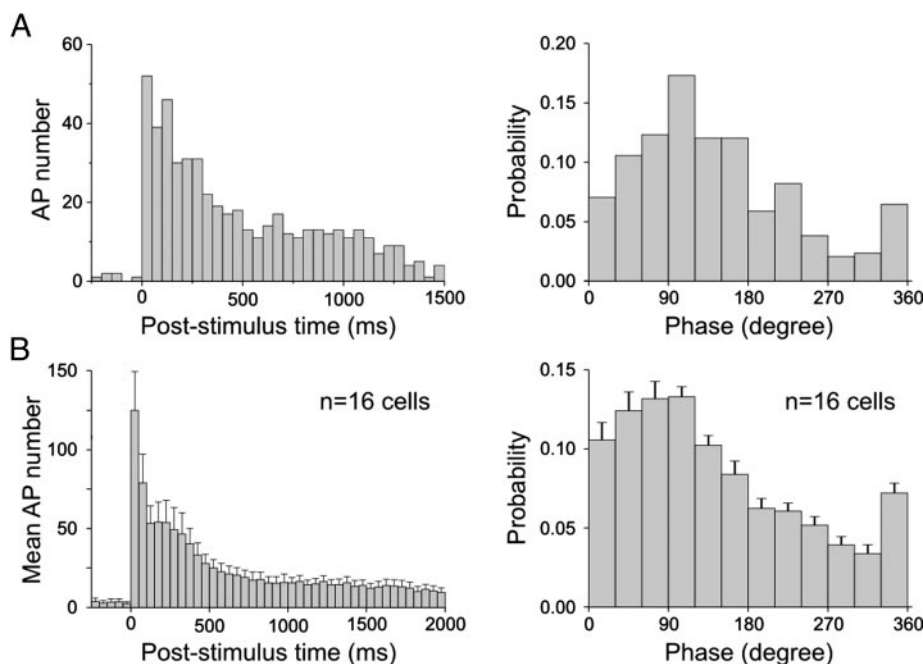


FIG. 5. Firing of MCs during network oscillations in OB slices. A: PSTH (left) and spike phase distribution (right) of the recorded cell presented in Fig. 4C ( $n = 826$  spikes in the PSTH,  $n = 212$  spikes for phase analysis). Vector length (equivalent to the O.I.) of the phase distribution is equal to 0.33, its angle to  $107.5^\circ$ ;  $P < 10^{-10}$ , Rayleigh's uniformity test. B: mean PSTH (left) and spike phasing (right) of 16 recorded cells. Mean vector length of the phase distribution,  $0.30 \pm 0.04$ ; mean angle,  $88.3 \pm 5.9^\circ$ ;  $P < 0.05$  in 2 cells,  $P < 10^{-3}$  in the others, Rayleigh's uniformity test.

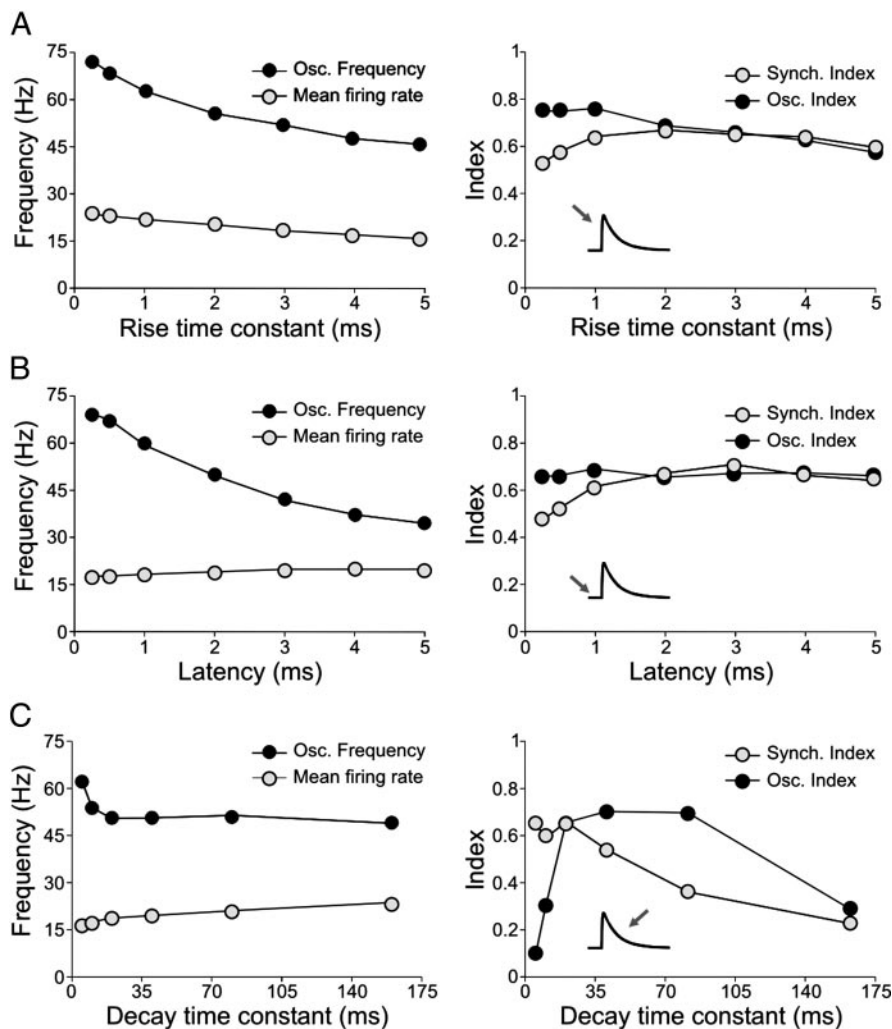


FIG. 6. Influence of time constants of lateral inhibition on I-network properties. In this model, MCs receive only lateral and recurrent inhibition. Note that a strong synchronization is present over a large range of parameters. *A, left*: plots of oscillation frequency (black circles) and the mean firing rate (gray circles) vs. the rise time constant of lateral inhibition. *A, right*: index of synchronization (gray circle) and of oscillation (black circle) vs. the rise time constant of lateral inhibition. *B*: plots of oscillation frequency and mean firing rate (*left*) and synchronization and oscillation indices (*right*) vs. the latency of lateral inhibition. *C*: plots of oscillation frequency and mean firing rate (*left*) and synchronization and oscillation indices (*right*) vs. the decay time constant. Network model contained recurrent and lateral inhibition described by smooth alpha functions. Excitatory input amplitude was set here to  $20 \text{ S/m}^2$ . For lateral and recurrent inhibition, amplitudes were adjusted according to time constants so that the total charge of coupling events remains constant. For the standard time constants (given in METHODS), amplitudes were 4 and  $16 \text{ S/m}^2$  for lateral and recurrent inhibition, respectively.

gamma frequencies. We then simulated a voltage-clamp experiment for pairs of MCs to further validate this model (Fig. 7D). We observed rise times for IPSPs very similar to those observed by Urban and Sakmann (2002) but we found that the latencies were different. This difference can be explained by the rise in global calcium levels in GCs (leading probably to lateral GABA release) needing sufficient presynaptic activation (Egger et al. 2005). Further experiments on this class of bulbar interneurons are required for a better understanding of their temporal integration.

#### Sensitivity of oscillation and synchronization to changes in the degree of inhibition

Because our results suggested that inhibition was the main key player involved in gamma oscillation, we built a network having asynchronous recurrent inhibition and asynchronous lateral inhibition to verify our general conclusions in a more realistic framework. We validated our second prediction (i.e., stability) by studying the effect on stability of global changes in inhibition strength. We subjected the model to proportional changes of both lateral and recurrent inhibition (Fig. 8A). With asynchronous GABA release, the oscillations were slightly reduced compared with smooth IPSCs (compare Fig. 3 with Fig. 8) but were closer to experimental data. This can be partly

explained by a large amount of synaptic noise in MCs (colored noise as opposed to the white noise that was injected into the modeled cells) being caused by the asynchronicity of the release that was not taken into account in our first approach.

When we increased the degree of inhibition, we observed a large reduction in the MC mean firing rate, from 105 to 17 Hz, whereas the oscillation frequency was only slightly decreased (from 89 to 57 Hz with a large plateau around 60 Hz, Fig. 8A, *left*). This reduction in firing rate was accompanied by an increase in MC synchrony (from 0.02 to 0.34, Fig. 8A, *right*), whereas the oscillation stability initially increased up to a peak at around  $0.02\text{--}0.03 \text{ S/m}^2$  before decreasing with stronger inhibition. We studied this experimentally by recording induced LFP oscillations in OB slices bathed with increasing concentrations of gabazine, a GABA<sub>A</sub> receptor antagonist (from 0.5 to  $20 \mu\text{M}$ ). We observed a large reduction in the firing of MCs (Fig. 8B, *top right*,  $n = 5$  for all concentrations; paired *t*-test with control conditions,  $P < 0.005$ ) with decreasing gabazine concentrations. However, the oscillation frequency remained constant (Fig. 8B, *top right*,  $n = 5$ , paired *t*-test,  $P > 0.2$ ), with the lowest oscillation frequency being  $64.7 \pm 2.7 \text{ Hz}$  for  $2 \mu\text{M}$  gabazine and the highest being  $68.2 \pm 4.3 \text{ Hz}$  for  $1 \mu\text{M}$  gabazine. The decrease in firing rate we observed with decreasing gabazine concentrations was accom-

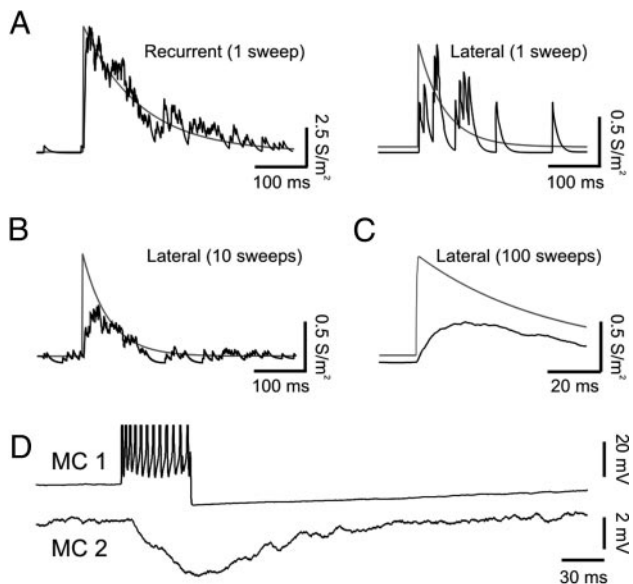


FIG. 7. Model of asynchronous  $\gamma$ -aminobutyric acid (GABA) release. *A, left*: inhibitory transients received by a MC after an action potential originating from the same cell (i.e., recurrent inhibition). A spike in a cell triggers an increase of the probability of receiving inhibitory events (red trace). Because of the high amplitude of the probability change, single events can barely be distinguished, even for a single trial. *A, right*: inhibitory transients received by a MC after an action potential in a neighboring cell (i.e., lateral inhibition). *B*: average of 10 repetitive inhibitory transients received by a MC after a single action potential in a neighboring cell. *C*: same as *B* but averaged over 100 repetitions and focused on the onset of the coupling. Whereas the probability of receiving inhibitory events increased almost instantaneously, the resulting current increased much more slowly (in the order of several milliseconds). *D*: lateral and recurrent synchronous inhibition illustrated by voltage traces of 2 simulated MCs (MC 1 and MC 2). *Top trace* shows the strong feedback inhibition occurring after a burst of spikes. *Bottom trace* shows the small deflection of the membrane voltage observed on a neighboring cell as a result of the burst in MC 1 [see Urban and Sakmann (2002) for a direct experimental comparison]. In *A, B, C*, and *D*, amplitudes of probability for asynchronous lateral and recurrent inhibition were 0.4 and  $4 \text{ ms}^{-1}$ , respectively. Unitary IPSC conductance was  $0.05 \text{ S/m}^2$ .

panied by an increase in synchronization of MCs. The S.I. increased from  $0.03 \pm 0.01$  ( $20 \mu\text{M}$  gabazine) to  $0.31 \pm 0.06$  (control) (Fig. 8*B*, bottom right,  $P < 0.005$  for 20 and  $2 \mu\text{M}$  and  $P < 0.05$  for  $1 \mu\text{M}$ ; paired *t*-test with control conditions). In these experiments, the O.I. was sensitive only to moderately high concentrations of gabazine ( $0.12 \pm 0.08$  and  $0.39 \pm 0.07$  for 20 and  $2 \mu\text{M}$ , respectively, compared with  $0.57 \pm 0.06$  for control conditions;  $P < 0.005$  and  $P < 0.05$ , respectively, with paired *t*-test). At low gabazine concentrations ( $1$  and  $0.5 \mu\text{M}$ ), the O.I. was unchanged ( $0.56 \pm 0.09$  and  $0.59 \pm 0.05$  compared with  $0.57 \pm 0.06$  for  $1$  and  $0.5 \mu\text{M}$  and control conditions, respectively; Fig. 8*B*, left traces and Fig. 8*B*, bottom right). In the presence of  $20 \mu\text{M}$  of gabazine, the O.I. after stimulation was not different from that from before stimulation (respectively,  $0.12 \pm 0.08$  and  $0.22 \pm 0.3$ ), indicating that the stimulation of sensory inputs did not induce oscillations. Values for the frequency, O.I., and S.I. from the model were close to those observed experimentally. The combination of theoretical and experimental approaches clearly demonstrates that lateral inhibition reliably generates evoked gamma oscillations in the OB circuit. Regarding lateral excitation, additional experiments need to be conducted to unambiguously demonstrate whether it plays only a minor role.

## DISCUSSION

Many features of our neuronal models are based on known properties of the mammalian OB network, in particular its basic architecture and synaptic organization. We found that in response to simulated ON inputs, MCs readily synchronize their firing and generate gamma oscillations. We were able to explain the particular kinetics of lateral inhibition necessary for inducing gamma oscillations (i.e., long latency and slow rise) as a result of the asynchronicity of GABA release from GC to MC. By contrast, increasing the strength of lateral inhibition did not affect the network oscillation frequency but enhanced MC synchronization. This latter finding was strongly supported by experimental results obtained from OB slice recordings. This study has provided new insights into the mechanisms that might regulate oscillatory synchrony by demonstrating the key role played by inhibitory interneurons in generating rhythms in the OB circuitry.

### Generating gamma oscillations in a neuronal network

Various mechanisms have been proposed to account for the generation of fast oscillations in neuronal networks. Previous studies focused particularly on the role of weak coupling. Weak couplings, whether they are excitatory (Van Vreewijk et al. 1994) or inhibitory (Wang and Buzsáki 1996), always require the intrinsic neuronal properties to be relatively homogeneous. However, this was not true for the OB network because the firing patterns were heterogeneous among MCs (see Fig. 4*D*, individual irregular firing pattern; Fig. 4*E*, mean firing frequency ranging from 15 to 66 Hz). Also, cell-to-cell variability limits the synchronization mechanisms that can be based on finely tuned subthreshold properties (e.g., Lampl and Yarom 1993). Indeed, the variability of the intrinsic MC oscillatory properties causes the resonant properties of the MC ensemble to disappear. For example, when we changed the mean subthreshold properties of the MCs in our model (e.g., resonance frequency) the oscillation frequency and quality of the network were not significantly affected (data not shown). Synchronization between MCs may also be triggered by a correlated, fast-fluctuating input (Hopfield and Brody 2003; Nikonov et al. 2002), although such oscillating inputs have so far never been reported in mammalian olfactory systems.

The precise nature of lateral excitation within the OB is not yet known. Therefore we assessed the role of excitatory coupling across a wide range of parameters, including brief excitatory couplings similar to those provided by gap junctions. Independent of these variations, the outputs of our network models were identical (see Supplementary Fig. 2). We always observed irregular firing and cycle skipping in the I-network and homogeneous firing without cycle skipping in the E-network. Thus given the particular characteristics of the OB network (i.e., slow lateral inhibition, cell-to-cell variability), we found that the effects of lateral inhibitory coupling dominate those of excitatory coupling in controlling the features of induced gamma oscillations.

### Mechanism of oscillations with irregular individual spiking

Gamma oscillations with a low individual spiking rate have been observed in the hippocampus of behaving rats (Bragin et al. 1995) and, more recently, in slices of rat hippocampus or

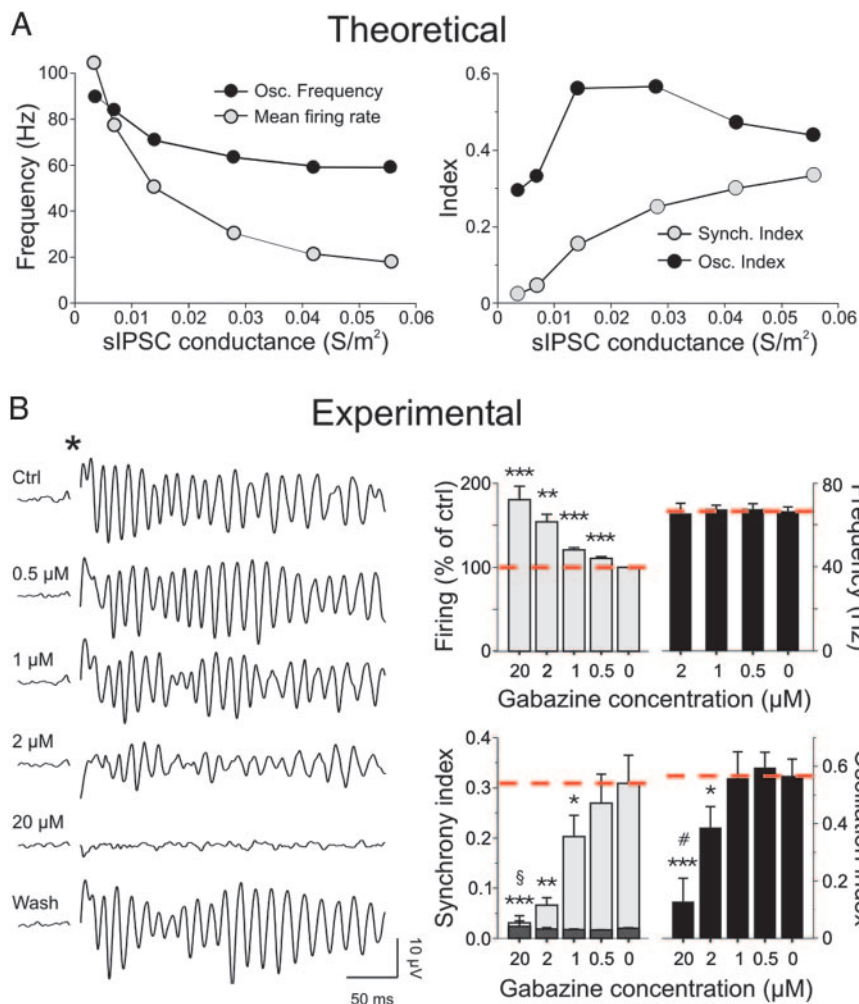


FIG. 8. Influence of lateral inhibition on MC firing and network oscillations. *A, left*: evolution of network oscillation (black circles) and mean individual firing rate (gray circles) frequencies of the inhibitory-coupled network when challenging the level of inhibition. *A, right*: evolution of oscillation (black circles) and synchronization (gray circles) indices of the inhibitory-coupled network when challenging the degree of inhibition. Amplitudes of probability for lateral and recurrent inhibition were 0.75 and  $7.5 \text{ ms}^{-1}$ , respectively. Slow kinetics were used for lateral inhibition (rise time of  $200 \mu\text{s}$  and decay time of  $10 \text{ ms}$ ). *B, left*: LFP recordings in the absence (Ctrl) and in the presence of various gabazine concentrations (0.5, 1, 2, and  $20 \mu\text{M}$ ). *B, top right*: histograms of MC population discharge (gray columns) and LFP oscillation frequency (black columns) in the absence or presence of different concentrations of gabazine. *B, bottom right*: evolution of synchrony (gray columns) and oscillation (black columns) indices with changes in gabazine concentration. Dashed lines indicate values obtained in the absence of the  $\text{GABA}_A$  antagonist. \* $P < 0.05$ ; \*\* $P < 0.005$ ; \*\*\* $P < 0.001$ ; §, not different from homogeneous distribution; #, not different from baseline (before the stimulation).

somatosensory cortex (Buhl et al. 1998; Fellous and Sejnowski 2000; Fisahn et al. 1998) using pharmacological manipulations. Previous detailed models of the hippocampus successfully reproduced these oscillations (e.g., Traub et al. 2001), but the mechanism generating population rhythm with irregularly spiking neurons is still unclear. In OB slices, no pharmacological agent is required to trigger gamma oscillations, which occur after activation of sensory fibers (see Figs. 4 and 8; Lagier et al. 2004). However, the similarity in frequency and individual firing rates between these studies and the present study suggests that the mechanisms underlying these two phenomena share some general features.

Brunel and Wang (2003) recently proposed that the oscillatory function might occur within the neuron population to explain fast oscillations with low individual firing rate. They propose that the oscillation occurs through instability of the firing rate (i.e., a Hopf bifurcation; see Brunel and Hakim 1999) as a result of the global negative feedback provided by lateral inhibition. The oscillation drives itself in the following way: at the peak of the oscillation a fraction of neurons (that can change randomly from cycle to cycle) fires and produces a large barrage of IPSPs within the entire population (because of the widespread connectivity). This barrage prevents most of the population firing for a while, thus creating the silent phase of the oscillation. Then, when the population is no longer laterally inhibited, a new fraction of neurons can fire and the

cycle starts again. This model predicted that synaptic time constants were crucial to the oscillation frequency as a result of the dominant role of lateral couplings. In a network of sparsely firing neurons that are coupled by inhibition, the frequency of the network oscillation depends on the latency and the rise time, but not on the decay time, of the inhibitory coupling. Indeed, we observed these predictions in our I-network model (see Fig. 6).

In the present study, our model gave new results concerning oscillation stability. After analyzing the role of the coupling amplitude and coupling time constants together for determining frequency, we showed that a network similar to that described by Brunel and Wang (2003) exhibited a remarkable oscillation frequency stability with respect to changes in coupling strength. We verified this in the OB, suggesting that gamma oscillations are a population phenomenon that occurs under the influence of lateral inhibition. However, further mathematical and experimental investigations are needed to understand how similar the bulbar gamma oscillations described here are to other known fast oscillations in the brain.

#### Potential roles for excitatory connections

MCs projecting to the same glomerulus are coupled by excitation with high probability (Urban and Sakmann 2002). Nevertheless, the mechanism of this excitatory stimulation is

still unclear. Some studies have reported a coupling through glutamate spillover (relying on *N*-methyl-D-aspartate receptors, see Carlson et al. 2000; or on  $\alpha$ -amino-3-hydroxy-5-methyl-4-isoxazolepropionic acid receptors, see Urban and Sakmann 2002), and others by an interaction between glutamate spillover and electrical coupling (Schoppa and Westbrook 2002). Glutamate spillover has also been suggested to take place between MC lateral dendrites (Isaacson 1999). Also, some local interneurons located in the GC layer have been reported as being excitatory (Didier et al. 2001). Despite the diversity of mechanisms and location of the coupling, we modeled a single source of lateral excitation (Fig. 2*B*). Lateral excitation generally improved the synchrony of oscillations generated by a dominant lateral inhibition (Fig. 2, *B* and *C*, *top traces*). A similar result has been found in a network coupled by inhibitory synapses in which gap junctions were added (Kopell and Ermentrout 2004; Traub et al. 2001). Nevertheless, experimental evidence is needed to support these predictions.

We noticed that the E-network had a tendency to oscillate at low frequencies (5–20 Hz). These rhythms may correspond to slow waves in cells connected to the same glomerulus (Schoppa and Urban 2003), suggesting that lateral excitation may play a role in slower rhythm generation. As excitatory connections between MCs mainly occur within a single glomerulus (Urban and Sakmann 2002), lateral excitation makes the functional units formed by individual glomeruli more homogeneous.

#### *Features of granule cell physiology*

The present work concludes to a central role of lateral inhibition in the generation and tuning of OB network gamma oscillations. Previous works described some properties of this lateral inhibition, that is, its independence toward sodium spikes, its long delay, and its long-lasting asynchronous release (e.g., Isaacson and Strowbridge 1998; Schoppa and Westbrook 1999; Urban and Sakmann 2002; reviewed in Schoppa and Urban 2003). GCs, the largest neuronal population in the OB circuit (Shepherd et al. 2004), can provide lateral inhibition in MCs through distinct mechanisms. First, MCs integrate IPSCs over long distances because of the length of their lateral dendrites, which in turn leads to a slow, asynchronous activation of a large number of GCs. Second, individual GC spines release GABA asynchronously as a result of prolonged high calcium levels or prolonged depolarization. Thus lateral inhibition features also depend on GC integration properties. However, little is known about the physiology of GCs despite a number of recent studies (Egger et al. 2005; Hall and Delaney 2002; Isaacson and Strowbridge 1998; Murphy et al. 2005; Schoppa and Westbrook 1999). In particular, their integration properties during network gamma oscillations are still unclear. We have shown that they do not induce somatic sodium spikes phase locked to the oscillations (Lagier et al. 2004). This suggests that the processing of MC inputs, which leads to their synchrony, is independent of the somatic spiking activity of GCs. A recent study in the OB of turtles revealed that GCs could generate  $\text{Na}^+$  spikes in their dendritic arborization (Pinato and Midtgaard 2005). Rall and Shepherd (1968) suggested that lateral inhibition could be supported by electrotonic propagation of GC inputs. Calcium spikes have also been proposed as a mechanism to support signal integration and GABA

release (Egger et al. 2005). Calcium dynamics appear to be a good candidate for explaining the asynchronicity of GABA release onto MCs. The threshold observed by Egger et al. (2005) in generating calcium spikes may be involved in the latency seen in the lateral inhibitory events recorded in pairs of MCs (Urban and Sakmann 2002) and may explain why only trains of MC spikes elicited lateral inhibitory events. We did not take this apparent nonlinearity in GC physiology into account in our model and therefore the long coupling latency was absent. However, MC pair recordings in magnesium-free solutions did not show any long latency (Isaacson and Strowbridge 1998). Therefore it seems reasonable to propose that during network oscillations, GCs receive massive inputs, and thus maintain high levels of calcium in the dendrites, which masks the nonlinearity of GC integration. More work on GC physiology, especially calcium dynamics, is needed to understand their contribution during network oscillations.

#### *Tuning inhibition for network plasticity*

Our results demonstrate that even if lateral inhibitory coupling between MCs is slow, fast oscillations still occur. Slow and long-lasting lateral inhibition may synchronize projection neurons on slow timescales, as seen in insects (Lei et al. 2002) and may contribute to dynamic slow changes in odor-evoked MC activity patterns, as seen in fish (Friedrich et al. 2004). Overall, our simulation over a large range of parameters showed that the same simple network architecture could lead to several dynamic states depending on the choice of the parameters. In particular, synchrony among a population of neurons can be adjusted by changes in inhibition strength without altering the global frequency. In principle, this could happen within local populations of neurons (such as a cluster of few glomeruli). Because changes in the degree of GC inhibition are linked to plasticity and learning (Lledo et al. 2005), we need to consider how learning can be included in our current model. For example, short-term plasticity of lateral inhibition can mediate the progressive synchronization of the neurons during repeated odor stimulation (e.g., for insects see Bazhenov et al. 2005; Stopfer et al. 1997). Irrespective of whether the plasticity affects the amplitude of unitary IPSCs or the probability of release, the consequences in the network will be similar.

#### *Making sense of spike timing*

Deciphering odor signals presents a common challenge to all animals. Interestingly, there are striking similarities between species in the organization of the olfactory pathway (Ache and Young 2005), indicating that many animals share general principles of odor information processing. Currently, it is well established that in mammals and nonmammalian vertebrates and homologous insect systems, both spatial (Leon and Johnson 2003) and temporal (Friedrich 2002; Laurent 2002) components of OB activity patterns convey sensory information (Friedrich and Stopfer 2001). However, it is unclear how these two dimensions are interrelated, despite all data supporting the presence of nonstatic activity patterns in the OB after odorant presentation. Fast oscillatory synchronization may have many roles in odor coding. Oscillations may integrate synaptic inputs over time to provide temporal formatting for the readout of activity patterns by preventing action potential firing for a

given period within each cycle. Oscillatory activity may also provide a clock signal for temporal coding. Alternatively, oscillations may help form functional neuronal assemblies. In insects, the information conveyed by the synchronization of projection neurons seems to be related to precise odors (Laurent 2002). However, in this model, categorization (i.e., the ability to link a specific odorant to a group or category of odorants) may not rely on spike synchrony (Sivan and Kopell 2004). By contrast, synchronous MC spikes seem to convey information about odor categories in vertebrates, the odor identity being conveyed by asynchronous spikes (Friedrich et al. 2004). Our results demonstrate that lateral inhibition mediates a regulatory function in temporal activity patterning in the OB and may therefore account for the distribution—in space and in time—of MC activity patterns in the coding space.

## APPENDIX

### Mathematical description of the single neuron

A single compartment that includes voltage-dependent currents described by Hodgkin–Huxley kinetics was used to model mitral cells. Their membrane potentials were calculated with the equations

$$C_m \frac{dV}{dt} = -\frac{1}{R_m} (V - E_L) - I_{Na} - I_{Kfast} - I_{Ka} - I_{Ks} - I_{NaP} - I_{syn} - I_{input} - I_{noise} \quad (A1)$$

where  $V$  is the membrane potential,  $C_m$  is the membrane capacitance,  $R_m$  is the input membrane resistance, and  $E_L$  is the leak reversal potential. All intrinsic currents were described by

$$I = g_{max} m^M h^H (V - E) \quad (A2)$$

where  $E$  denotes the reversal potential of the current and  $g_{max}$  is its maximal conductance. The gating variables  $m$  and  $h$  follow the differential equations

$$dm/dt = (m_\infty - m)\tau_m \quad (A3)$$

$$dh/dt = (h_\infty - h)\tau_h \quad (A4)$$

or equivalently

$$dm/dt = a_m(1 - m) - b_m m \quad (A5)$$

$$dh/dt = a_h(1 - h) - b_h h \quad (A6)$$

Channel conductance was described using the time- and voltage-gating variables  $m$  and  $h$  ( $M$  and  $H$  represent the number of activating and inactivating gates, respectively). The following equations were used.

### $Ka$

- $M = H = 1$
- $\tau_m(V) = 25 \exp[(V + 45)/13.3] / \{\exp[(V + 45)/10] + 1\}$
- $\tau_h(V) = 55.5 \exp[(V + 70)/5.1] / \{\exp[(V + 70)/5] + 1\}$
- $m_\infty = 1 / \{\exp[-(V - 70)/14] + 1\}$
- $h_\infty = 1 / \{\exp[(V + 47.4)/6] + 1\}$

### $Ks$

- $M = H = 1$
- $\tau_m(V) = 10$
- $\tau_h(V) = 2000 + 220 / \{\exp[-(V + 71.6)/6.85] + 1\}$

- $m_\infty = 1 / \{\exp[-(V + 34)/6.5] + 1\}$
- $h_\infty = 1 / \{\exp[(V + 65)/6.6] + 1\}$

### $NaP$

- $H = 1$
- $m(V) = 1 / \{\exp[-(V + 51)/5] + 1\}$

### $Kfast$

- $M = 2$
- $H = 1$

For Kfast kinetics we used the tables available from the Senselab databank (<http://senselab.med.yale.edu>) and adapted from Bhalla and Bower (1993).

### $Na$

- $M = 3$
- $H = 1$
- $a_m = 0.32(V + 50) / \{1 - \exp[-(V + 50)/4]\}$
- $b_m = 0.28(V + 23) / \{\exp[(V + 23)/5] - 1\}$
- $a_h = 0.128 / \exp[(V + 46)/18]$
- $b_h = 4 / \{1 + \exp[-(V + 23)/5]\}$

## ACKNOWLEDGMENTS

We thank B. Gutkin, R. Friedrich, M. Richardson, and M. Grubb for helpful discussions on the manuscript.

Present address of B. Bathellier: Laboratory of Computational Neuroscience, Brain and Mind Institute, Ecole Polytechnique Fédérale de Lausanne, Bât. AA-B, CH-1015 Lausanne, Switzerland.

## GRANTS

This work was supported by the Fédération pour la Recherche sur le Cerveau.

## REFERENCES

- Ache BW and Young JM.** Olfaction: diverse species, conserved principles. *Neuron* 48: 417–430, 2005.
- Adrian ED.** Olfactory reactions in the brain of the hedgehog. *J Physiol* 100: 459–473, 1942.
- Adrian ED.** The electrical activity of the mammalian olfactory bulb. *Electroencephalogr Clin Neurophysiol* 2: 377–388, 1950.
- Balu R, Larimer P, and Strowbridge BW.** Phasic stimuli evoke precisely timed spikes in intermittently discharging mitral cells. *J Neurophysiol* 92: 743–753, 2004.
- Bazhenov M, Stopfer M, Sejnowski TJ, and Laurent G.** Fast odor learning improves reliability of odor responses in the locust antennal lobe. *Neuron* 46: 483–492, 2005.
- Bhalla US and Bower JM.** Exploring parameter space in detailed single cell models: simulations of the mitral and granule cells of the olfactory bulb. *J Neurophysiol* 69: 1948–1965, 1993.
- Bischofberger J and Jonas P.** Action potential propagation into the presynaptic dendrites of rat mitral cells. *J Physiol* 504: 359–365, 1997.
- Bragin A, Jando G, Nadasdy Z, Hetke J, Wise K, and Buzsáki G.** Gamma (40–100 Hz) oscillation in the hippocampus of the behaving rat. *J Neurosci* 15: 47–60, 1995.
- Brunel N and Hakim V.** Fast global oscillations in networks of integrate-and-fire neurons with low firing rates. *Neural Comput* 11: 1621–1671, 1999.
- Brunel N and Wang XJ.** What determines the frequency of fast network oscillations with irregular neural discharges? I. Synaptic dynamics and excitation–inhibition balance. *J Neurophysiol* 90: 415–430, 2003.
- Buhl EH, Tamas G, and Fisahn A.** Cholinergic activation and tonic excitation induce persistent gamma oscillations in mouse somatosensory cortex in vitro. *J Physiol* 513: 117–126, 1998.
- Carlson GC, Shipley MT, and Keller A.** Long-lasting depolarizations in mitral cells of the rat olfactory bulb. *J Neurosci* 20: 2011–2021, 2000.

- Castillo PE, Carleton A, Vincent JD, and Lledo P-M. Multiple and opposing roles of cholinergic transmission in the main olfactory bulb. *J Neurosci* 19: 9180–9191, 1999.
- Chen WR and Shepherd GM. Membrane and synaptic properties of mitral cells in slices of rat olfactory bulb. *Brain Res* 745: 189–196, 1997.
- Christie JM, Bark C, Hormuzdi SG, Helbig I, Monyer H, and Westbrook GL. Connexin36 mediates spike synchrony in olfactory bulb glomeruli. *Neuron* 46: 761–772, 2005.
- Davison AP, Feng J, and Brown D. A reduced compartmental model of the mitral cell for use in network models of the olfactory bulb. *Brain Res Bull* 51: 393–399, 2000.
- Desmaisons D, Vincent JD, and Lledo P-M. Control of action potential timing by intrinsic subthreshold oscillations in olfactory bulb output neurons. *J Neurosci* 19: 10727–10737, 1999.
- Didier A, Carleton A, Bjaalie JG, Vincent J-D, Ottersen OP, Storm-Mathisen J, and Lledo P-M. A dendrodendritic reciprocal synapse provides a recurrent excitatory connection in the olfactory bulb. *Proc Natl Acad Sci USA* 98: 6441–6446, 2001.
- Egger V, Svoboda K, and Mainen ZF. Mechanisms of lateral inhibition in the olfactory bulb: efficiency and modulation of spike-evoked calcium influx into granule cells. *J Neurosci* 23: 7551–7558, 2003.
- Egger V, Svoboda K, and Mainen ZF. Dendrodendritic synaptic signals in olfactory bulb granule cells: local spine boost and global low-threshold spike. *J Neurosci* 25: 3521–3530, 2005.
- Fellous J and Sejnowski TJ. Cholinergic induction of oscillations in the hippocampal slice in the slow (0.5–2 Hz), theta (5–12 Hz) and gamma bands. *Hippocampus* 10: 187–197, 2000.
- Fisahn A, Pike FG, Buhl EH, and Paulsen O. Cholinergic induction of network oscillations at 40 Hz in the hippocampus in vitro. *Nature* 394: 186–189, 1998.
- Freeman WJ. *Mass Action in the Nervous System*. New York: Academic Press, 1975.
- Freeman WJ. Simulation of chaotic EEG patterns with a dynamic model of the olfactory system. *Biol Cybern* 56: 139–150, 1987.
- Friedrich RW and Stopfer M. Recent dynamics in olfactory population coding. *Curr Opin Neurobiol* 11: 468–474, 2001.
- Friedrich RW. Real time odor representations. *Trends Neurosci* 25: 487–489, 2002.
- Friedrich RW, Habermann CJ, and Laurent G. Multiplexing using synchrony in the zebrafish olfactory bulb. *Nat Neurosci* 7: 862–871, 2004.
- Hall BJ and Delaney KR. Contribution of a calcium-activated non-specific conductance to NMDA receptor-mediated synaptic potentials in granule cells of the frog olfactory bulb. *J Physiol* 543: 819–834, 2002.
- Hopfield JJ and Brody CD. Separating objects and “neural” computation. *C R Biol* 326: 219–222, 2003.
- Hutcheon B and Yarom Y. Resonance, oscillation and the intrinsic frequency preferences of neurons. *Trends Neurosci* 23: 216–222, 2000.
- Isaacson JS. Glutamate spillover mediates excitatory transmission in the rat olfactory bulb. *Neuron* 23: 377–384, 1999.
- Isaacson JS and Strowbridge BW. Olfactory reciprocal synapses: dendritic signalling in the CNS. *Neuron* 20: 749–761, 1998.
- Kay LM. Two species of gamma oscillations in the olfactory bulb: dependence on behavioral state and synaptic interactions. *J Integr Neurosci* 2: 31–44, 2003.
- Kopell N and Ermentrout B. Chemical and electrical synapses perform complementary roles in the synchronization of interneuronal networks. *Proc Natl Acad Sci USA* 101: 15482–15487, 2004.
- Lagier S, Carleton A, and Lledo P-M. Interplay between local GABAergic interneurons and relay neurons generates gamma oscillations in the rat olfactory bulb. *J Neurosci* 24: 4382–4392, 2004.
- Lampl I and Yarom Y. Subthreshold oscillations of the membrane potential: a functional synchronizing and timing device. *J Neurophysiol* 70: 2181–2186, 1993.
- Laurent G. Olfactory network dynamics and the coding of multidimensional signals. *Nat Rev Neurosci* 3: 884–895, 2002.
- Laurent G, Stopfer M, Friedrich RW, Rabinovich MI, Volkovskii A, and Abarbanel HDI. Odor encoding as an active, dynamical process: experiments, computation, and theory. *Annu Rev Neurosci* 24: 263–297, 2001.
- Lei H, Christensen TA, and Hildebrand JG. Local inhibition modulates odor-evoked synchronization of glomerulus-specific output neurons. *Nat Neurosci* 5: 557–565, 2002.
- Leon M and Johnson BA. Olfactory coding in the mammalian olfactory bulb. *Brain Res Rev* 42: 23–32, 2003.
- Li Z and Hopfield JJ. Modeling the olfactory bulb and its neural oscillatory processes. *Biol Cybern* 61: 379–392, 1989.
- Linster C and Hasselmo M. Modulation of inhibition in a model of olfactory bulb reduces overlap in the neural representation of olfactory stimuli. *Behav Brain Res* 84: 117–127, 1997.
- Lledo P-M, Gheusi G, and Vincent JD. Information processing in the mammalian olfactory system. *Physiol Rev* 85: 281–317, 2005.
- Martin C, Gervais R, Hugues E, Messaoudi B, and Ravel N. Learning modulation of odor-induced oscillatory responses in the rat olfactory bulb: a correlate of odor recognition? *J Neurosci* 24: 389–397, 2004.
- Migliore M, Hines ML, and Shepherd GM. The role of distal dendritic gap junctions in synchronization of mitral cell axonal output. *J Comput Neurosci* 18: 151–161, 2005.
- Murphy GJ, Darcy DP, and Isaacson JS. Intraglomerular inhibition: signaling mechanisms of an olfactory microcircuit. *Nat Neurosci* 8: 354–364, 2005.
- Neville KR and Haberly LB. Beta and gamma oscillations in the olfactory system of the urethane-anesthetized rat. *J Neurophysiol* 90: 3921–3930, 2003.
- Nikonov AA, Parker JM, and Caprio J. Odorant-induced olfactory receptor neural oscillations and their modulation of olfactory bulb responses in the channel catfish. *J Neurosci* 22: 2352–2362, 2002.
- Nusser Z, Kay LM, Laurent G, Homanics GE, and Mody I. Disruption of GABA<sub>A</sub> receptors on GABAergic interneurons leads to increased oscillatory power in the olfactory bulb network. *J Neurophysiol* 86: 2823–2833, 2001.
- Pinato G and Midtgaard J. Dendritic sodium spikelets and low-threshold calcium spikes in turtle olfactory bulb granule cells. *J Neurophysiol* 93: 1285–1294, 2005.
- Rall W and Shepherd GM. Theoretical reconstruction of field potentials and dendrodendritic synaptic interactions in olfactory bulb. *J Neurophysiol* 31: 884–915, 1968.
- Richardson MJE, Brunel N, and Hakim V. From subthreshold to firing-rate resonance. *J Neurophysiol* 89: 2538–2554, 2003.
- Schoppa NE, Kinzie JM, Sahara Y, Segerson TP, and Westbrook GL. Dendrodendritic inhibition in the olfactory bulb is driven by NMDA receptors. *J Neurosci* 18: 6790–6802, 1998.
- Schoppa NE and Urban NN. Dendritic processing within olfactory bulb circuits. *Trends Neurosci* 26: 501–506, 2003.
- Schoppa NE and Westbrook GL. Regulation of synaptic timing in the olfactory bulb by an A-type potassium current. *Nat Neurosci* 2: 1106–1113, 1999.
- Schoppa NE and Westbrook GL. AMPA autoreceptors drive correlated spiking in olfactory bulb glomeruli. *Nat Neurosci* 5: 1194–1202, 2002.
- Shepherd GM, Wei RC, and Greer CA. Olfactory bulb. In: *The Synaptic Organization of the Brain* (5th ed.), edited by Shepherd GM. Oxford, UK: Oxford Univ. Press, 2004, p. 165–216.
- Shipley MT and Ennis M. Functional organization of olfactory system. *J Neurobiol* 30: 123–176, 1996.
- Sivan E and Kopell N. Mechanism and circuitry for clustering and fine discrimination of odors in insects. *Proc Natl Acad Sci USA* 101: 17861–17866, 2004.
- Stopfer M, Bhagavan S, Smith BH, and Laurent G. Impaired odor discrimination on desynchronization of odor-encoding neural assemblies. *Nature* 390: 70–74, 1997.
- Teyke T and Gelperin A. Olfactory oscillations augment odor discrimination not odor identification by Limax CNS. *Neuroreport* 10: 1061–1068, 1999.
- Traub R, Kopell N, Bibbig A, Buhl EH, le Beau FEN, and Whittington MA. Gap junctions between interneuron dendrites can enhance synchrony of gamma oscillations in distributed networks. *J Neurosci* 21: 9478–9486, 2001.
- Urban NN and Sakmann B. Reciprocal intraglomerular excitation and intra- and interglomerular lateral inhibition between mouse olfactory bulb mitral cells. *J Physiol* 542: 355–367, 2002.
- van Vreeswijk C, Abbott L, and Ermentrout GB. When inhibition not excitation synchronises neural firing. *J Comput Neurosci* 1: 313–321, 1994.
- Wang X-J. Ionic basis for intrinsic 40 Hz neuronal oscillations. *Neuroreport* 5: 221–224, 1993.
- Wang X-J and Buzsáki G. Gamma oscillation by synaptic inhibition in a hippocampal interneuronal network model. *J Neurosci* 16: 6402–6413, 1996.
- Wang XY, McKenzie JS, and Kemm RE. Whole-cell K<sup>+</sup> currents in identified olfactory bulb output neurones of rats. *J Physiol* 490: 63–77, 1996.

Volume 95, April 2006

Pages 2678–2691: Bathellier B, Lagier S, Faure P, and Lledo P-M. “Circuit Properties Generating Gamma Oscillations in a Network Model of the Olfactory Bulb” (doi:10.1152/jn.01141.2005; <http://jn.physiology.org/cgi/content/full/95/4/2678>). During production, some material in Table 1 was misrepresented. Corrected Table 1 is presented here.

TABLE 1. Parameters of MC network architecture

General Cell Properties												
$C_m$	Membrane capacitance					Eq. 1*			0.01 F/m <sup>2</sup>			Bhalla and Bower 1993
$R_m$	Membrane resistance					Eq. 1			10 Ωm <sup>2</sup>			Bhalla and Bower 1993
$E_l$	Reverse leak potential					Eq. 1			−66.5 mV			Bhalla and Bower 1993
Conductances		$Na$		$NaP$		$K_{fast}$		$Ka$		$Ks$		
$M$	Number of activating gates	Eq. 2	3	Bhalla and Bower 1993	1	Wang 1993	2	Bhalla and Bower 1993	1	~	1	~
$H$	Number of inactivating gates	Eq. 2	1	Bhalla and Bower 1993	0 (no inactivation)	Wang 1993	1	Bhalla and Bower 1993	1	~	1	~
$g_{max}$	Averaged maximal conductance	Eq. 2	500 S/m <sup>2</sup>	Bhalla and Bower 1993	1.1 S/m <sup>2</sup>	#	500 S/m <sup>2</sup>	Bhalla and Bower 1993	100 S/m <sup>2</sup>	#	310 S/m <sup>2</sup>	#
$E$	Reversal potential	Eq. 2	45 mV	Bhalla and Bower 1993	45 mV	Bhalla and Bower 1993	−70 mV	Bhalla and Bower 1993	−70 mV	Bhalla and Bower 1993	−70 mV	Bhalla and Bower 1993
$\tau_m$	Activation time constant	Eq. 3	Function; see Ref.	Bhalla and Bower 1993	0 (instantaneous activation)	Wang 1993	Function; see Ref.	Bhalla and Bower 1993	See METHODS	Wang 1996	10	#
$\tau_h$	Inactivation time constant	Eq. 4	Function; see Ref.	Bhalla and Bower 1993	Not used (no inactivation)	Wang 1993	Function; see Ref.	Bhalla and Bower 1993	See METHODS	Wang 1996	See METHODS	Wang 1993
$m_4$	Steady-state activation	Eq. 3	Function; see Ref.	Bhalla and Bower 1993	Function; see Ref.	Wang 1993	Function; see Ref.	Bhalla and Bower 1993	See METHODS	Wang 1996	See METHODS	Wang 1993
$h_4$	Steady-state inactivation	Eq. 4	Function; see Ref.	Bhalla and Bower 1993	Not used (no inactivation)	Wang 1993	Function; see Ref.	Bhalla and Bower 1993	See METHODS	Wang 1996	See METHODS	Wang 1993
Synaptic transients			Excitation (auto and lateral)				Recurrent inhibition			Lateral inhibition		
$\tau_l$	Latency		1.4 ms	Urban and Sakmann 2002; Schoppa and Westbrook 1999		1 ms	Varied, data not shown		2 ms	Varied in Fig. 8		
$\tau_r$	Rise time constant	Eq. 7	0.5 ms	Brunel and Wang 2003		1 ms	Varied, data not shown		3 ms	Varied in Fig. 8		
$\tau_d$	Decay time constant	Eq. 7	10 ms	Varied, data not shown		50 ms	Varied, data not shown		20 ms	Varied in Fig. 8		
$E_{reversal}$	Reversal potential	Eq. 8	0 mV	Brunel and Wang 2003; Bower 1993		−70 mV	Brunel and Wang 2003		−70 mV	Brunel and Wang 2003		
$g_{syn}$	Maximum conductance	Eq. 8	0–1.6 S/m <sup>2</sup>	Varied in Fig. 3		0–64 S/m <sup>2</sup>	Varied in Fig. 3		0–32 S/m <sup>2</sup>	Varied in Fig. 3		
Connectivity												
$L$	Characteristic distance					Eq. 9			4–5 cells			Varied, data not shown
$G(d)$	Connection probability					Eq. 9			See METHODS			Function arbitrarily chosen
Probabilistic synaptic description												
$P_{max\ recurrent}$	Maximum transient probability								7.5 ms <sup>−1</sup>			Inferred from Isaacson and Strowbridge 1998
$P_{max\ lateral}$	Maximum transient probability								0.75 ms <sup>−1</sup>			Inferred from Isaacson and Strowbridge 1998
$P_o$	Basal probability								0.0125 ms <sup>−1</sup>			Castillo et al. 1999
$\tau_l$	Latency								0.5 ms			Inferred from Isaacson and Strowbridge 1998
$\tau_r$	Rise time constant								0.5 ms			Inferred from Isaacson and Strowbridge 1998
$\tau_d$	Decay time constant (for rec. inh.)								150 ms			Inferred from Isaacson and Strowbridge 1998
$\tau_d$	Decay time constant (for lat. inh.)								50 ms			Inferred from Isaacson and Strowbridge 1998

Downloaded from jn.physiology.org on October 21, 2008

TABLE 1. (continued)

Individual uIPSC			
$\tau_l$	Latency	0 ms	No latency needed
$\tau_r$	Rise time constant	0.5 ms	Brunel and Wang 2003
$\tau_d$	Decay time constant	10 ms	Castillo et al. 1999
$g_{\text{syn}}$	Maximum conductance	0–0.06 S/m <sup>2</sup>	Varied in Fig. 5

\*Values from this column refer to equations in METHODS and the APPENDIX. #, these parameters control membrane subthreshold oscillations. In the absence of experimental values, we chose these values to fit subthreshold oscillation properties with experimental data. ~, <http://senselab.med.yale.edu>.

Also during production, *Eqs. A3 and A4* of the APPENDIX were misrepresented. The correct equations are presented here.

$$dm/dt = (m_{\infty} - m)/\tau_m \quad (\text{A3})$$

$$dh/dt = (h_{\infty} - h)/\tau_h \quad (\text{A4})$$